ACS APPLIED NANO MATERIALS

www.acsanm.org

Letter

Surface Wrinkling with Memory for Programming Adhesion and Wettability

Feng Wang, Senbo Xiao, Sihai Luo, Yuequn Fu, Bjørn Helge Skallerud, Helge Kristiansen, Mengkui Cui, Chao Zhong, Siqi Liu, Yizhi Zhuo, Jianying He,* and Zhiliang Zhang*

Cite This: https://doi.org/10.1021/acsanm.2c05410

Read Online

ACCESS | Metrics & More | Article Recommendations | Supporting Information

ABSTRACT: Modulating surface wrinkling is important for a variety of engineering applications. It has been known for more than two decades that the wavelength of surface wrinkles occurring in a metal film−soft polymer system scales linearly with the deposited film thickness. In the current experimental study of ultrathin gold film (0.2−8 nm) deposition on polydimethylsiloxane (PDMS), an unexplored thickness-dependent wrinkling phenomenon is found. By manipulating the deposition sequence as a degree of freedom for tailoring surface topography, we discovered a morphology memory effect where the wrinkle evolution in the subsequent deposition step inherits the surface pattern already formed in the previous step. Moreover, a stepwise deposition targeting 1 nm thick film can lead to 1 order of magnitude higher surface roughness than the one in the continuous deposition. By programming the sequences within 8 nm Au deposition, a surface strain map varying drastically from 0.2% to 27% is realized. Instructed by the strain map, we show the great potentials of tailored wrinkles in alternating surface wettability, enhancing surface Raman scattering, and on-demand tuning of surface adhesion.

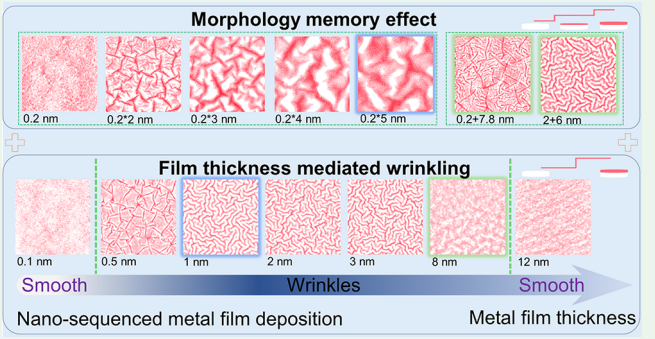

KEYWORDS: *surface wrinkling, wrinkles, stepwise deposition, morphology memory effect, surface adhesion*

INTRODUCTION

Wrinkled surfaces are widely observed in nature[1,2] and find applications in polymer systems, including triboelectric nanogenerators,[3] photovoltaics,[4] stretchable electronics,[5] organic light-emitting diodes (OLEDs),[6] smart adhesives,[7] and so on. Surface wrinkling occurs when the compressive stress generated in a hard layer due to property mismatch with a soft substrate reaches a critical buckling stress.[8,9] Modifications of soft materials by means of plasma treatment,[10] ultraviolet/ozone (UVO) radiation,[11] ion beam irradiation,[12] and metal deposition[8,13,14] are often applied to form the hard film layer and to wrinkle the surface. Among these methods, metal deposition that can accurately control the deposition thickness is frequently used.

Bowden et al. investigated the wrinkles caused by thermal contraction after metal deposition and established eqs 1 and 2 to estimate the critical stress (σ_{crit}) for wrinkle formation and the wavelength (L) of the formed wrinkles, respectively[8]

$$\sigma_{crit} \approx 0.52\left(\frac{E_m}{(1-\nu_m^2)}\right)^{1/3}\left(\frac{E_p}{(1-\nu_p^2)}\right)^{2/3} \quad (1)$$

$$L \approx 4.36t\left(\frac{E_m(1-\nu_p^2)}{E_p(1-\nu_m^2)}\right)^{1/3} \approx 4.4t\left(\frac{E_m}{E_p}\right)^{1/3} \quad (2)$$

where E is the Young's modulus, subscripts m and p refer to the metal film and the soft polymer substrate, respectively, ν is the Poisson's ratio, and t is the deposited film thickness. These equations have been widely used in studying surface wrinkles and their correlation with the film properties.[15−17] Generally, as indicated in eq 2, the wavelength of wrinkles for a specific metal deposition on polymer increases linearly with the increase of film thickness.[18,19] However, in the case of ultrathin (subnano/nanoscale) Au film deposition on polydimethylsiloxane (PDMS), we observe an unexpected phenomenon, especially in the case with stepwise deposition. The wavelength of wrinkles remained constant with increasing Au thickness. We also find an interesting memory effect in discontinuous stepwise depositions of 0.2−8 nm Au film on PDMS. The

Received: December 17, 2022
Accepted: February 28, 2023

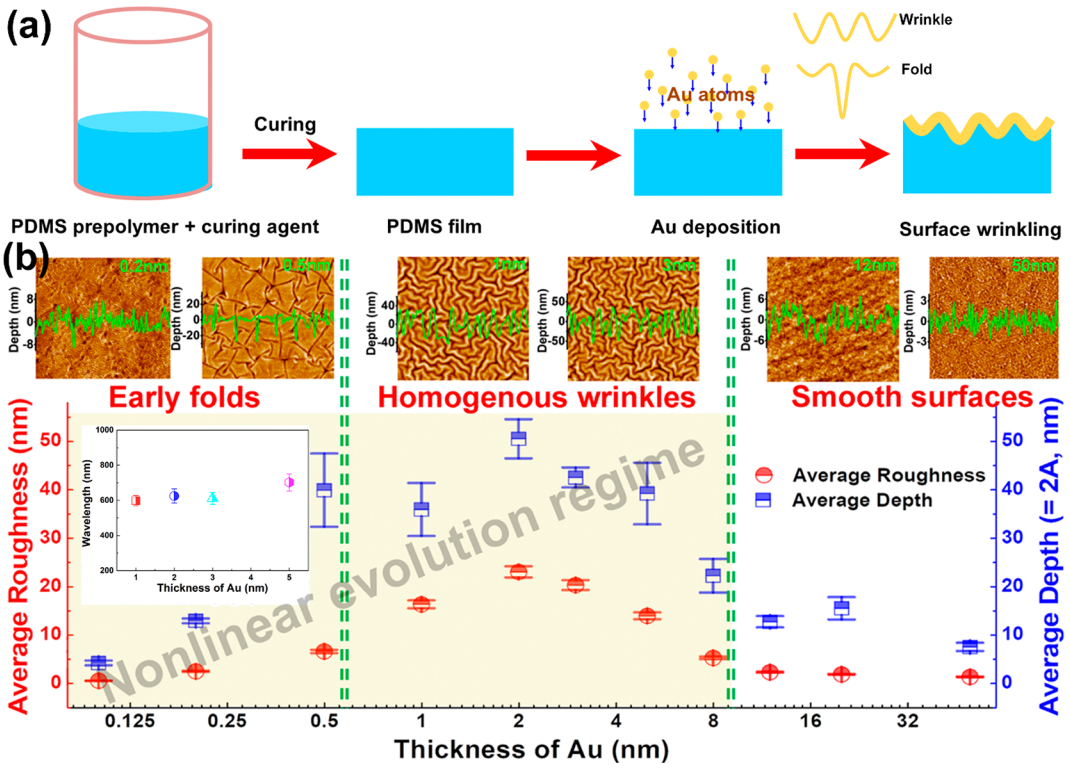

Figure 1. The procedure of creating surface wrinkles and nonlinear evolution of surface wrinkling in ultrathin Au deposition. (a) A schematic diagram shows the process of fabricating surface wrinkles. (b) The main curve shows the average roughness and average depth (= 2*A*, *A* is the amplitude of the wave) of the surface structures as a function of film thickness. The curves inserted are the wavelength of surfaces with homogeneous labyrinth-like wrinkles. The wavelength of wrinkles remains almost constant from 1 to 5 nm deposition. Combined with the AFM morphologies, the evolution process of "early folds−homogenous wrinkles−smooth surfaces" is detected; the folds are deep crevices with more highly localized curvatures than wrinkles. The green curves inserted in the AFM show the depth distribution along the line profiles from the midsections of the AFM images. The size of the AFM images is 10 × 10 μm^2.

wrinkle patterns in subsequent steps "remember" what occurred in the previous deposition steps. Moreover, with folds generated at the first step, the stress concentration in these regions can lead to unique wrinkle-to-fold transition and fold-reorganization during further deposition. Therefore, the nanoscale sequence of deposition can act as a new parameter for programming surface topography. We also show the potentials of nanosequenced deposition in tailoring surface adhesion, surface wettability, and surface Raman scattering.

RESULTS AND DISCUSSION

Film-Thickness-Dependent Wrinkling. The classical wrinkling mechanism indicates that the wavelength of wrinkle evolves linearly with the increase of the deposited film thickness once a critical stress is reached. In the case of depositing ultrathin Au film on PDMS with a Young's modulus of 203 kPa, we find an unexpected wrinkling behavior, as shown in Figure 1. The PDMS surface is initially smooth (indicated by the Supplementary Figure S8). During the increase of Au thickness, the surface roughness monotonically increases until a maximum is reached at 2 nm thick Au deposition. Interestingly, further deposition decreases the roughness, and the surface returns to be smooth again once the deposited Au thickness is above 8 nm. The surface morphology can be characterized as a three-stage evolution process, that is, early folds−homogeneous wrinkles−smooth surfaces. The smoothness of surfaces after 8 nm suggests the stress generated during deposition is below the level necessary for onset of surface wrinkling. B. Osmani et al. has showed the vanish of wrinkles after Au sputtering, but the underlying mechanism of the phenomena here remains undiscovered.[17] When the deposited Au film thickness is in the range of 0.2−8 nm, a unique regime where wrinkling occurs and evolves nonlinearly along with film thickness is discovered. The exact mechanism behind this interesting observation remains to be described in detail. However, assuming the temperature field is not significantly influenced by the ultrathin film deposition, the wrinkling phenomenon which is governed by the elastic modulus of the deposited film may be attributed to the reported size effect where the elastic modulus of ultrathin film becomes higher than that of the film with thickness beyond 8 nm. Alternatively, the non-homogenous metal layer in the early stage of the deposition has a more extended surface area/effective higher interatomic spacing than in bulk metal which will cause a built-in strain in the film, hence leading to unusual wrinkling. On the other hand, the interfacial layer between metal film and PDMS substrate can also play an essential role.[8]

In the wrinkling process reported above, the deposited Au film first appears as particle clusters. When 0.2 nm Au is deposited, wrinkles start to appear along with folds. The folds are generated when the surface is compressed beyond one-third of the initial wrinkle wavelength.[20,21] Neighboring wrinkles finally annihilate and form deep folds with highly localized curvatures. When the Au thickness reaches 0.5 nm, the folds continue to grow and the surface transforms into locally folded parts coexisting with flat regions, forming a multiperiodic pattern.[21] A continuous Au film layer starts to form on the surface, and homogeneous shallow wrinkles

https://doi.org/10.1021/acsanm.2c05410
ACS Appl. Nano Mater. XXXX, XXX, XXX−XXX

caused by uniform compressive stress appear after 1 nm Au is deposited. Generally, the wavelength of labyrinth-like wrinkles is assumed to increase linearly along with film thickness.[8,18,19] The wavelength of wrinkles after depositing 5 nm Au should be 5 times than that after depositing 1 nm Au as eq 2 suspected. However, in our experiment the wavelength of the wrinkles remains approximately constant in the deposition interval of 1−5 nm (Figure 1b). The periodicity of the wrinkles (wavelength) is calculated using a 2D fast Fourier transform (2D FFT) analysis of the related atomic force microscopy (AFM) image. A detailed comparison between the calculated wavelength evolution from eq 2 and the wavelength in this work is given in Supplementary Figure S7. Although it remains a challenge to explain the unusual evolution because of lacking effective methods for measuring the mechanical properties of both ultrathin metal films and interfacial layers, the nonlinear evolution regime can offer a number of possibilities for engineering of the surface topography.

Morphology Memory Effect. In addition to the thickness-dependent wrinkling phenomenon, we find that deposition sequence offers another unexplored freedom to tailor the surface morphology. In order to attain a target film thickness, we can deposit the metal continuously as the approach used above, or use a discontinuous stepwise method, namely, depositing layers of specified thicknesses with cooling steps in between. We use the stepwise deposition with an equal step size (thickness) of 1 nm to form 8 nm thick Au film on PDMS. Unlike the continuous deposition where the wrinkles disappeared and surface smoothness recovered when the film thickness reaches 8 nm, it is surprising to find that the wrinkles continue to evolve, and the pattern in the subsequent step "remembers" the one already formed in the previous steps (Figure 2 and Supplementary Figure S9). We name this finding as a morphology memory effect. In the 1 nm stepwise deposition, the similarity of the patterns is evidenced by both the morphology and wavelength of the wrinkles. The surface roughness and amplitude evolve with the increase of film thickness. The amplitudes of the wrinkles increase at first and then decrease after 8 nm Au is deposited. This agrees with the observation above that the compressive stress developed in the 8 nm Au film is below the critical wrinkling stress. Further deposition will then decrease the amplitudes of the wrinkles. Despite the changes in the amplitudes, the morphology and wavelength of the wrinkles have been "memorized".

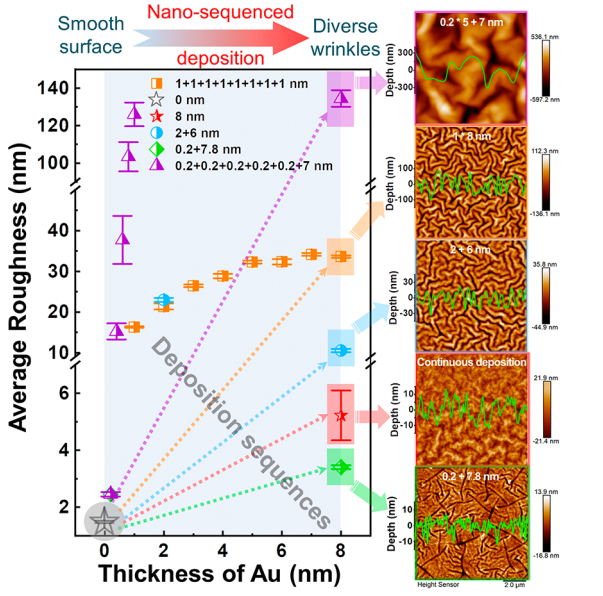

Figure 2. The morphology memory effect. The main curve shows the average roughness of the wrinkling structures as a function of film thickness in various nanosequenced depositions. The inserted AFM images show the surface morphologies after 8 nm Au is deposited by various sequences. The green curves inserted in the AFM show the depth distribution along the line profiles from the midsections of the AFM images. The size of the AFM images is 10 × 10 μm^2.

The morphology memory effect is further demonstrated by two alternative two-step discontinuous depositions: (1) an initial 2 nm step with a subsequent 6 nm step and (2) an initial 0.2 nm step followed by a 7.8 nm step on PDMS (Figure 2). We observe that in both cases the final morphologies inherit the patterns that occurred in the previous deposition steps. The striking morphology memory effect could have great potential for creating deterministic wrinkle structures and can also be applied in thin film property measurement.[22] In another nanosequence of depositing 0.2 nm Au for 5 cycles at first and then depositing a subsequent 7 nm step, a surface with extremely high roughness and amplitude is observed. The first 0.2 nm step and the subsequent subnano sequences combined with the morphology memory effect lead to extraordinary wrinkling evolution, which will be discussed in detail in the following section. As indicated in Figure 2, a wide range of tunable roughness (3.4−134.5 nm) can be achieved in depositing 8 nm Au through different stepwise depositions, in contrast to the roughness (5.2 nm) achieved in continuous deposition. Therefore, the stepwise deposition provides a new degree of freedom for programming surface structures by carefully manipulating the first subnano/nano layer deposition and the subsequent deposition sequence. Different sequences can not only shape the surface morphology but also regulate the surface roughness and wrinkle amplitudes.

Sequence Intensified Wrinkling. We further show that discontinuous deposition with subnano step sizes can drastically alter the surface deformation. The wrinkling deformation with subnano sequence deposition is enhanced by initial folds and the morphology memory effect. For instance, depositing a target 1 nm film, the discontinuous deposition with equal step sizes of 0.2 nm for 5 cycles creates a giant surface deformation, compared with the continuous deposition. Figure 3a shows the surface morphologies in each step which are remarkably different from that shown in Figure 1, indicating that initial folds uniquely coin the surface structure evolution. The morphology memory is characterized by a special fan-like texture, a triangle center connected by three folds. Focusing on the "fan", the evolution of the fan-like texture clearly points out the growth and expansion of the folds. Once a fold appears, the compressive stress and subsequent deformation will be localized in the fold areas.[20,23] Therefore, in the stepwise deposition with equal step sizes of 0.2 nm, the initial folds after 0.2 nm deposition will localize the stress, and the "fan" keeps growing in both width and depth in the subsequent deposition, creating a giant deformation. A unique wrinkle-to-fold transition and fold-reorganization are observed from the surface topography. The regions isolated by the folds show wrinkles at the very beginning of the deposition (Figure 3a and 3c). The wrinkles finally disappear after 1 nm Au has been deposited, because the strain greatly localizes into the folds and therefore relaxes the deformation in their neighborhood. The phenomena observed

https://doi.org/10.1021/acsanm.2c05410
ACS Appl. Nano Mater. XXXX, XXX, XXX−XXX

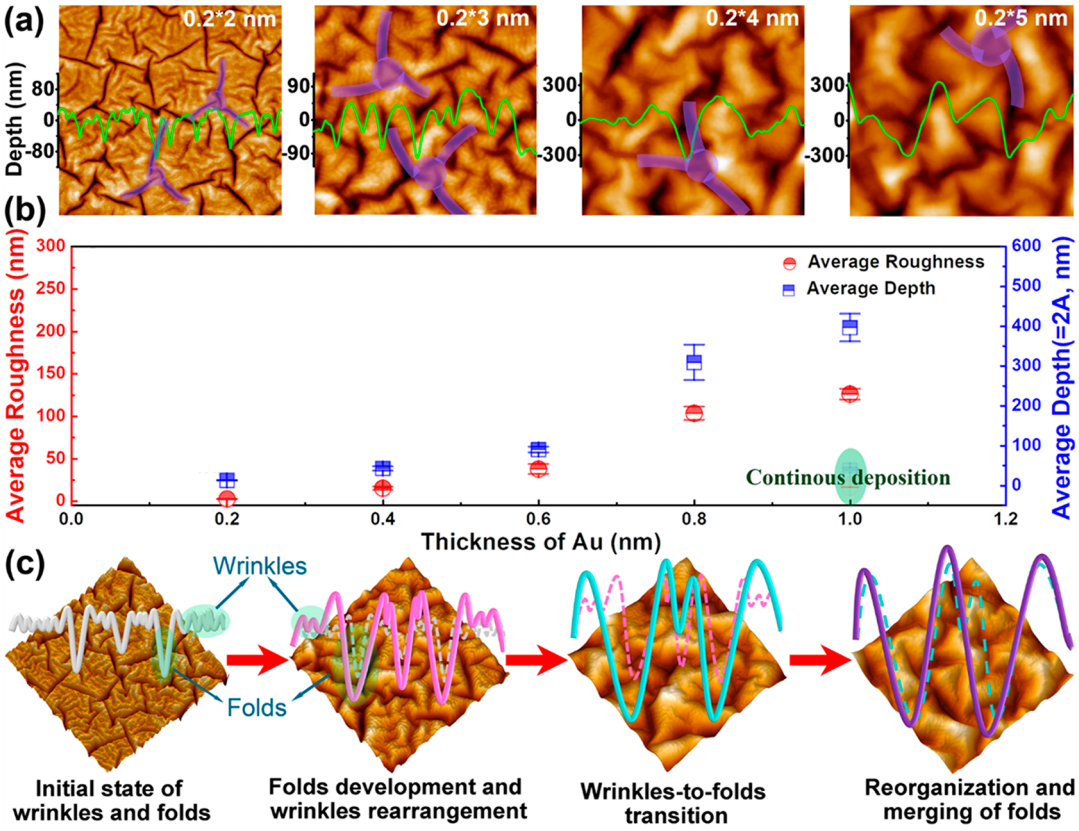

Figure 3. Subnano sequence intensified wrinkling. (a) Surface morphology evolutions during a stepwise deposition. The Au is deposited 0.2 nm by 0.2 nm up to 1 nm. The green curves inserted are the depth distribution along the line profiles from the midsections of the AFM images. The fan-like morphology evolution is indicated by the violet marks. (b) The data points show the average roughness and average depth of the surfaces as functions of the thickness. (c) The schematic diagram combined with 3D AFM images shows the topography evolution in this model. Both wrinkle-to-fold transition and fold-reorganization are observed. The size of all the AFM images is 10 × 10 μm^2.

here agree with the reported wrinkle-to-fold transition by Stone et al.[21] Besides, this fold propagation not only eliminates the wrinkles on the ridges but also merges small ridges and folds to form larger ridges and folds, namely, fold-reorganization. The evolution of the surface waves is illustrated in Figure 3c. The wrinkle-to-fold transition and the newly discovered fold-reorganization therefore result in a huge surface deformation. We note nearly 1 order of magnitude higher roughness and amplitude are generated in this subnano stepwise deposition compared to that of the continuous deposition (Figure 3b). Here we show another possibility of using nanosequenced deposition in programming surface wrinkles through amplifying fold patterns with memory.

Applications of the New Surface Programming Freedom. Surface strain is a parameter that can be used to characterize the surface topographical properties including roughness and wavelength. Figure 4a summarizes the compressive strains calculated using the method given in the inserted image[21] and presented as functions of deposition thickness and deposition sequences within 8 nm Au. Programming wrinkles through modulating substrate elasticity has been widely reported;[15] however, the diverse topographies manipulated by nanosequenced deposition are unprecedented and presented here for the first time. The surface strains cover a wide range from 0.2% to 27% which enable great flexibility for guiding the design of multiple wrinkles/folds by ultrathin metal deposition. The strain map shown in Figure 4a is divided into four domains. The domains "early folds" and "labyrinthic wrinkling" represent two distinct morphologies in continuous deposition. The "early folds" represents the morphologies with folds in subnano metal deposition. The "labyrinthic wrinkling" indicates the homogeneous wrinkles through continuous deposition of 1−8 nm Au. The stepwise deposition leads to widely tunable surface strains with the domains "labyrinthic wrinkling with memory" and "memory-driven and folds intensified wrinkling". The "labyrinthic wrinkling with memory" implies the surface morphologies that evolve following the labyrinthic wrinkles in the primary step, while the "memory-driven and folds intensified wrinkling" describes the surface wrinkles that are patterned by the folds in the first deposition step. The morphology memory effect in stepwise deposition results in a special freedom for surface programming. Through modulating deposition sequences and film thickness, it is possible to achieve diverse wrinkling behaviors that generally do not occur in microscale deposition.[8] More surface topographies can be expected by coupling the prestructured surface, elasticity and thickness of PDMS, and other parameters with nanosequenced deposition.

Finally, we demonstrate that tailored surface wrinkling at different domains can lead to various applications. Au with 1, 2, and 3 nm thickness is deposited targeting two types of morphology, i.e., the surfaces with labyrinthic wrinkles (continuous deposition) and the surfaces with folds intensified wrinkles (discontinuous deposition with equal step sizes of 0.2 nm). Controlled smooth surfaces without wrinkles are also introduced as references (details of fabrication are given in the

https://doi.org/10.1021/acsanm.2c05410
ACS Appl. Nano Mater. XXXX, XXX, XXX−XXX

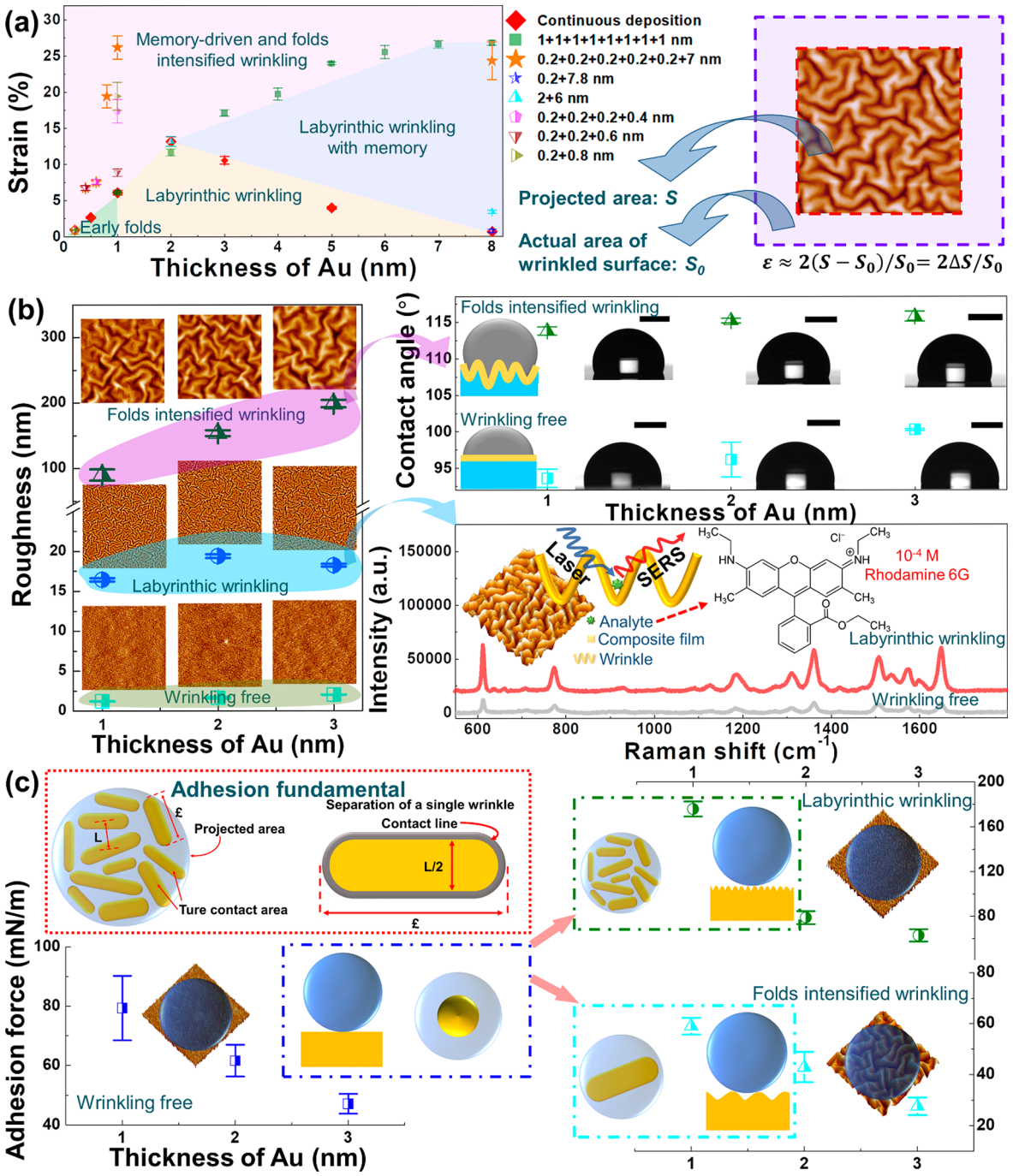

Figure 4. Programmable surface strain maps and applications of programmed wrinkling behaviors. (a) Drastically different surface strains can be programmed as functions of deposition thickness and deposition sequences within 8 nm Au. The inserted image shows the method used for calculating the strain. Four distinctive strain domains are identified. (b) Roughness and morphology of programmed wrinkling within 3 nm Au deposition are first shown. "Folds intensified wrinkling" implies the surface with 0.2 nm step size, "labyrinthic wrinkling" implies the surface with continuous deposition, and "wrinkling free" implies reference surfaces without wrinkles. The folds intensified wrinkling and labyrinthic wrinkling show potentials in improving surface hydrophobicity and enhancing surface Raman scattering, respectively. (c) The "on-demand adhesion tuning" can be realized on PDMS surfaces through tailoring surface wrinkling behaviors. The adhesion contact line of surface to adhesives can be increased through program labyrinthic wrinkling and decreased through program folds intensified wrinkling. The size of all the AFM images inserted is 20 × 20 μm^2.

Experimental Section). As shown in Figure 4b, distinct surface roughness and morphology are obtained through controlling sequences in 3 nm Au deposition. The "folds intensified wrinkling" produces a surface with high roughness, which holds potential for making liquid-repellent surfaces. The "folds intensified wrinkling" can transfer the wetting behaviors of droplets on surfaces from Young's mode to Wenzel's mode[23,24] and increase the water contact angle (WCA) to more than ~115° from around ~90° on smooth surfaces (Figure 4b). Interestingly, the "labyrinthic wrinkling" creates an excellent plasmon effect under Raman scattering; it thus can potentially be applied to flexible, transparent, and large-scale film for

https://doi.org/10.1021/acsanm.2c05410
ACS Appl. Nano Mater. XXXX, XXX, XXX−XXX

enhancing the detected signal of analyte. We carry out the surface-enhanced Raman spectroscopy (SERS) test on the "labyrinthic wrinkling" and "wrinkling free" surfaces both after 3 nm deposition. A typical Raman probe molecule rhodamine 6G (R6G) is used to demonstrate the SERS activity of the wrinkled substrate in comparison with the flat substrate. As shown in Figure 4b, distinctive Raman peaks of R6G appear at 612 and 1509 cm^{-1}.[25,26] The labyrinthic wrinkled substrate exhibits significant enhancement (with enhancement factors of 3.5 and 4.5 for peaks at 612 and 1509 cm^{-1}, respectively) of the characteristic Raman peak intensity of R6G at 10^{-4} M with respect to the flat substrate. The unique wrinkle-enhanced SERS is mainly attributed to the presence of subnano/nanoscale gaps in the labyrinthic wrinkles and thus the generation of hot spots.

Eventually, we show the special on-demand adhesion tuning of the PDMS surface through deposition sequence tailored wrinkling. Surfaces with patterns have been widely observed in nature for controlling adhesion and release.[27] Attempts to mimic natural systems and design surface geometry for smart adhesion is a popular topic.[28] However, efficient and scalable methods that can tune the adhesion of surfaces in a broad range remain a challenge. Here in this work, smart adhesives are achieved by simply changing the thickness and sequences of deposited Au film. The adhesion force needed to separate a spherical probe from surfaces is closely related to the contact line between the probe and the surfaces. As indicated in Figure 4c, the contact line of a single wrinkle at separation can be simply defined by its perimeter $L + 2\pounds$ (L and $\pounds$ are the wavelength of the wrinkle and the length at contact, respectively).[29] The real contact area between the wrinkled surface and the probe highly depends on the number of wrinkles in contact, that is, the wavelength of wrinkles. To increase the adhesion, wrinkles with a small wavelength on the surface are desired. To decrease the adhesion, wrinkles with a large wavelength on the surface will be good choices. Therefore, as shown in Figure 4c, surface adhesion can either be enhanced through tailoring "labyrinthic wrinkling" or be reduced through enabling "folds intensified wrinkling". The thickness of Au can act as another parameter for adjusting the adhesion force, because the adhesion energy of the interface decreases with increasing Au thickness (more detailed discussions are given in Supplementary Section 7). Through controlling Au thickness (1, 2, and 3 nm) and deposition sequences, the adhesion forces on wrinkled surfaces are tuned in a much wider scope of 28−176 mN/m compared with 47−79 mN/m on smooth surfaces (Figure 4c). Therefore, the nanosequenced metal deposition provides an accessible method for on-demand adhesion tuning and can attract broad interests.

CONCLUSIONS

In this work, we experimentally show that there are alternative pathways to modulate the surface morphology by controlling the nano/subnano deposition sequences. In a stepwise deposition, we observe a morphology memory effect where the instability response in the first step dictates the subsequent wrinkle evolution. By programming different sequences to obtain a total of 8 nm Au deposition, drastically different surface wrinkles are obtained. In a stepwise deposition with initial folds, an interesting wrinkle-to-fold and fold-reorganization phenomenon is shown, which leads to intensified surface deformation. Using the nanosequenced deposition as a surface programming freedom, various promising applications including alternating surface wettability, enhancing surface Raman scattering, and on-demand surface adhesion tuning are demonstrated. Through tuning the nanoscale Au thickness (1, 2, and 3 nm) and deposition sequences, the adhesion forces on wrinkled surfaces can be adjusted in a wide range of 28−176 mN/m. The widely tunable instability response also suggests ultrathin modification layers can play essential roles in fabricating various metal−polymer systems for stretchable and wearable electronics. Last but not the least, programming wrinkles in ultrathin film deposition opens new avenues for nanofabrication.

EXPERIMENTAL SECTION

Materials Synthesis. Polydimethylsiloxanes (PDMSs) with different elasticities are synthesized as soft substrates in the bilayer system. PDMS prepolymer (Sylgard 184, Dow Corning) and curing agent are mixed in a weight ratio of 10:1. The final mixtures are degassed in a vacuum chamber and then placed at room temperature (20 °C) for 51 h to obtain cured PDMS. To achieve PDMS with higher Young's modulus for programming surfaces without wrinkles in Figure 4, samples after curing for 50 h are transferred into an oven of 100 °C and held for 1 h. The thickness of all PDMSs is controlled as 1.82 ± 0.02 mm.

Metal Deposition. PDMSs are cut into a size of 1 cm × 1 cm and put into the vacuum chamber of a sputter coater (208 HR B, Cressington) incorporated with an MTM-20 High Resolution Thickness Controller for sputtering deposition; the resolution of the controller is better than 0.1 nm. The metal target is ∼60 mm above the sample surfaces. Metal targets of Au are used in this work. The argon gas pressure and sputtering current are fixed at 0.02 mbar and 20 mA. The tooling factor of the MTM-20 controller used is 1.8. The density for Au deposition is 19.30 g/cm^3. The sputtering rate is 0.15 nm/s. For the continuous deposition, targeted Au thickness is deposited before cooling down and taking out the sample. For the stepwise deposition, the sample is deposited to a specific thickness of Au first; after a time interval of 5 min, another Au layer will be deposited. The sample will be taken out of the chamber until the targeted Au thickness is reached.

Characterization. The mechanical properties of PDMS are measured through quasi-static nanoindentation tests in a TriboIndenter 950 (Hysitron, Inc.) by using a cylindrical diamond flat punch with 53.70 ± 0.06 μm diameter. Thicknesses of the PDMS are measured by a digimatic micrometer (Mitutoyo, ID-C112GB). The surface morphologies and three-dimensional information are recorded by an atomic force microscope (AFM, Dimension Icon, Bruker) using ScanAsyst in air mode. The average roughness, average depth, and wavelength are calculated from AFM images using the methods described in the Supplementary Section 5. The water contact angle is measured by a drop shape analyzer (DSA100, KRÜSS). An AFM colloidal probe technique is used to measure the adhesion force and adhesion energy between the colloidal sphere and surfaces. The tests are proceeded at room temperature in water using an Asylum MFP-3D AFM (Asylum Research).[30] Raman spectra are tested using a Renishaw confocal Raman spectrometer with laser excitation wavelength at 532 nm. The laser beam is focused onto the sample through an objective lens (×50) with selected 0.5 mW laser power and 10 s acquisition time. To prepare for surface-enhanced Raman scattering (SERS) measurement, the samples are immersed in the aqueous solution of rhodamine 6G at a concentration of 10^{-4} M for about 4 h. The samples are then rinsed with ethanol and dried using a N_2 stream before the measurement.

ASSOCIATED CONTENT

Supporting Information

The Supporting Information is available free of charge at https://pubs.acs.org/doi/10.1021/acsanm.2c05410.

https://doi.org/10.1021/acsanm.2c05410
ACS Appl. Nano Mater. XXXX, XXX, XXX−XXX

Statistical analysis, mechanical properties of PDMS, quality of Au films, wrinkle formation process, average depth and wavelength calculation, tailoring surface morphologies through initial wrinkling, and wrinkle controlled surface applications (PDF)

AUTHOR INFORMATION

Corresponding Authors

Jianying He − *Department of Structural Engineering, Norwegian University of Science and Technology (NTNU), Trondheim 7491, Norway;* orcid.org/0000-0001-8485-7893; Email: jianying.he@ntnu.no

Zhiliang Zhang − *Department of Structural Engineering, Norwegian University of Science and Technology (NTNU), Trondheim 7491, Norway;* orcid.org/0000-0002-9557-3455; Email: zhiliang.zhang@ntnu.no

Authors

Feng Wang − *Department of Structural Engineering, Norwegian University of Science and Technology (NTNU), Trondheim 7491, Norway; Foshan (Southern China) Institute for New Materials, Foshan 528231, China; Shenzhen Adventure Tech Co., Ltd., Shenzhen 518000, China;* orcid.org/0000-0002-6112-2824

Senbo Xiao − *Department of Structural Engineering, Norwegian University of Science and Technology (NTNU), Trondheim 7491, Norway*

Sihai Luo − *Department of Chemistry, Norwegian University of Science and Technology (NTNU), Trondheim 7491, Norway;* orcid.org/0000-0001-5614-9734

Yuequn Fu − *Department of Structural Engineering, Norwegian University of Science and Technology (NTNU), Trondheim 7491, Norway*

Bjørn Helge Skallerud − *Department of Structural Engineering, Norwegian University of Science and Technology (NTNU), Trondheim 7491, Norway*

Helge Kristiansen − *Department of Structural Engineering, Norwegian University of Science and Technology (NTNU), Trondheim 7491, Norway*

Mengkui Cui − *School of Physical Science and Technology, ShanghaiTech University, Shanghai 201210, China*

Chao Zhong − *Center for Materials Synthetic Biology, Shenzhen Institute of Synthetic Biology and CAS Key Laboratory of Quantitative Engineering Biology, Shenzhen Institute of Synthetic Biology, Shenzhen Institutes of Advanced Technology, Chinese Academy of Sciences, Shenzhen 518055, China;* orcid.org/0000-0002-6638-3652

Siqi Liu − *Department of Structural Engineering, Norwegian University of Science and Technology (NTNU), Trondheim 7491, Norway*

Yizhi Zhuo − *Department of Structural Engineering, Norwegian University of Science and Technology (NTNU), Trondheim 7491, Norway;* orcid.org/0000-0003-1415-3561

Complete contact information is available at: https://pubs.acs.org/10.1021/acsanm.2c05410

Notes

The authors declare no competing financial interest.

ACKNOWLEDGMENTS

The Research Council of Norway is acknowledged for the support to the FRIPRO project Towards Design of Super-Low Ice Adhesion Surfaces (SLICE, 250990), the PETROMAKS project Durable Arctic Icephobic Materials (AIM, 255507), the support to the Norwegian Micro- and Nano-Fabrication Facility, NorFab (245963/F50), and the support to the NANO2021 project Dual-Functional Anti-Gas Hydrate Surfaces (DAndra, 302348).

REFERENCES

(1) Tallinen, T.; Chung, J. Y.; Rousseau, F.; Girard, N.; Lefèvre, J.; Mahadevan, L. On the growth and form of cortical convolutions. *Nat. Phys.* **2016**, *12* (6), 588.

(2) Liang, H.; Mahadevan, L. The shape of a long leaf. *Proc. Natl. Acad. Sci. U. S. A.* **2009**, *106* (52), 22049−22054.

(3) Ahn, J.; Zhao, Z.-J.; Choi, J.; Jeong, Y.; Hwang, S.; Ko, J.; Gu, J.; Jeon, S.; Park, J.; Kang, M. Morphology-controllable wrinkled hierarchical structure and its application to superhydrophobic triboelectric nanogenerator. *Nano Energy* **2021**, *85*, 105978.

(4) Kim, J. B.; Kim, P.; Pégard, N. C.; Oh, S. J.; Kagan, C. R.; Fleischer, J. W.; Stone, H. A.; Loo, Y.-L. Wrinkles and deep folds as photonic structures in photovoltaics. *Nat. Photonics* **2012**, *6* (5), 327.

(5) Lee, G.; Zarei, M.; Wei, Q.; Zhu, Y.; Lee, S. G. Surface Wrinkling for Flexible and Stretchable Sensors. *Small* **2022**, *18* (42), 2203491.

(6) Li, Y.; Kovačič, M.; Westphalen, J.; Oswald, S.; Ma, Z.; Hänisch, C.; Will, P.-A.; Jiang, L.; Junghaehnel, M.; Scholz, R. Tailor-made nanostructures bridging chaos and order for highly efficient white organic light-emitting diodes. *Nat. Commun.* **2019**, *10* (1), 2972.

(7) Wang, D.; Xu, L.; Zhang, L.; Zhang, L.; Zhang, A. Hydrophobic/superhydrophobic reversible smart materials via photo/thermo dual-response dynamic wrinkled structure. *Chem. Eng. J.* **2021**, *420*, 127679.

(8) Bowden, N.; Brittain, S.; Evans, A. G.; Hutchinson, J. W.; Whitesides, G. M. Spontaneous formation of ordered structures in thin films of metals supported on an elastomeric polymer. *Nature* **1998**, *393* (6681), 146.

(9) Wang, Y.; Liu, Q.; Zhang, J.; Hong, T.; Sun, W.; Tang, L.; Arnold, E.; Suo, Z.; Hong, W.; Ren, Z. Giant Poisson's Effect for Wrinkle-Free Stretchable Transparent Electrodes. *Adv. Mater.* **2019**, *31*, 1902955.

(10) Tan, A.; Pellegrino, L.; Cabral, J. o. T. Tunable Phase Gratings by Wrinkling of Plasma-Oxidized PDMS: Gradient Skins and Multiaxial Patterns. *ACS Appl. Polym. Mater.* **2021**, *3* (10), 5162−5170.

(11) Cai, Y.-W.; Zhang, X.-N.; Wang, G.-G.; Li, G.-Z.; Zhao, D.-Q.; Sun, N.; Li, F.; Zhang, H.-Y.; Han, J.-C.; Yang, Y. A flexible ultra-sensitive triboelectric tactile sensor of wrinkled PDMS/MXene composite films for E-skin. *Nano Energy* **2021**, *81*, 105663.

(12) Lee, J. H.; Jeong, H.-C.; Won, J.; Kim, D. H.; Lee, D. W.; Song, I. H.; Oh, J. Y.; Kim, D.-H.; Liu, Y.; Seo, D.-S. Formation of the Wrinkle Structure on a Styrene−Butadiene−Styrene Block Copolymer Surface by Surface Chemical Reformation via Ion-Beam Irradiation. *J. Phys. Chem. C* **2020**, *124* (15), 8378−8385.

(13) Zhu, T.; Wu, K.; Xia, Y.; Yang, C.; Chen, J.; Wang, Y.; Zhang, J.; Pu, X.; Liu, G.; Sun, J. J. N. L. Topological Gradients for Metal Film-Based Strain Sensors. *Nano Lett.* **2022**, *22* (16), 6637−6646.

(14) Yu, S.; Guo, Y.; Li, H.; Lu, C.; Zhou, H.; Li, L. J. A. A. M. Interfaces. *Tailoring Ordered Wrinkle Arrays for Tunable Surface Performances by Template-Modulated Gradient Films.* **2022**, *14* (9), 11989−11998.

(15) Das, A.; Banerji, A.; Mukherjee, R. Programming feature size in the thermal wrinkling of metal polymer bilayer by modulating substrate viscoelasticity. *ACS Appl. Mater. Interfaces* **2017**, *9* (27), 23255−23262.

(16) Stafford, C. M.; Harrison, C.; Beers, K. L.; Karim, A.; Amis, E. J.; VanLandingham, M. R.; Kim, H.-C.; Volksen, W.; Miller, R. D.;

https://doi.org/10.1021/acsanm.2c05410
ACS Appl. Nano Mater. XXXX, XXX, XXX−XXX

Simonyi, E. E. A buckling-based metrology for measuring the elastic moduli of polymeric thin films. *Nature materials* **2004**, *3* (8), 545−550.
(17) Osmani, B.; Deyhle, H.; Töpper, T.; et al. Gold layers on elastomers near the critical stress regime[J]. *Advanced Materials Technologies* **2017**, *2* (10), 1700105.
(18) Wu, K.; Yuan, H.; Li, S.; Zhang, J.; Liu, G.; Sun, J. Two-stage wrinkling of Al films deposited on polymer substrates. *Scripta Materialia* **2019**, *162*, 456−459.
(19) Khang, D.-Y.; Jiang, H.; Huang, Y.; Rogers, J. A. A stretchable form of single-crystal silicon for high-performance electronics on rubber substrates. *Science* **2006**, *311* (5758), 208−212.
(20) Pocivavsek, L.; Dellsy, R.; Kern, A.; Johnson, S.; Lin, B.; Lee, K. Y. C.; Cerda, E. Stress and fold localization in thin elastic membranes. *Science* **2008**, *320* (5878), 912−916.
(21) Kim, P.; Abkarian, M.; Stone, H. A. Hierarchical folding of elastic membranes under biaxial compressive stress. *Nature materials* **2011**, *10* (12), 952.
(22) Yin, J.; Yagüe, J. L.; Eggenspieler, D.; Gleason, K. K.; Boyce, M. C. Deterministic order in surface micro-topologies through sequential wrinkling. *Advanced materials* **2012**, *24* (40), 5441−5446.
(23) Brau, F.; Vandeparre, H.; Sabbah, A.; Poulard, C.; Boudaoud, A.; Damman, P. Multiple-length-scale elastic instability mimics parametric resonance of nonlinear oscillators. *Nat. Phys.* **2011**, *7* (1), 56.
(24) Feng, X.; Jiang, L. Design and creation of superwetting/antiwetting surfaces. *Adv. Mater.* **2006**, *18* (23), 3063−3078.
(25) Jung, K.; Hahn, J.; In, S.; Bae, Y.; Lee, H.; Pikhitsa, P. V.; Ahn, K.; Ha, K.; Lee, J. K.; Park, N. Hotspot-engineered 3D multipetal flower assemblies for surface-enhanced Raman spectroscopy. *Adv. Mater.* **2014**, *26* (34), 5924−5929.
(26) Lin, D.; Wu, Z.; Li, S.; Zhao, W.; Ma, C.; Wang, J.; Jiang, Z.; Zhong, Z.; Zheng, Y.; Yang, X. Large-area Au-nanoparticle-functionalized Si nanorod arrays for spatially uniform surface-enhanced Raman spectroscopy. *ACS Nano* **2017**, *11* (2), 1478−1487.
(27) Autumn, K.; Liang, Y. A.; Hsieh, S. T.; Zesch, W.; Chan, W. P.; Kenny, T. W.; Fearing, R.; Full, R. J. Adhesive force of a single gecko foot-hair. *Nature* **2000**, *405* (6787), 681−685.
(28) Brodoceanu, D.; Bauer, C.; Kroner, E.; Arzt, E.; Kraus, T. Hierarchical bioinspired adhesive surfaces—a review. *Bioinspiration & biomimetics* **2016**, *11* (5), No. 051001.
(29) Chan, E. P.; Smith, E. J.; Hayward, R. C.; Crosby, A. J. Surface wrinkles for smart adhesion. *Adv. Mater.* **2008**, *20* (4), 711−716.
(30) Cui, M.; Wang, X.; An, B.; Zhang, C.; Gui, X.; Li, K.; Li, Y.; Ge, P.; Zhang, J.; Liu, C. Exploiting mammalian low-complexity domains for liquid-liquid phase separation−driven underwater adhesive coatings. *Science advances* **2019**, *5* (8), eaax3155.

https://doi.org/10.1021/acsanm.2c05410
ACS Appl. Nano Mater. XXXX, XXX, XXX−XXX